Microwave-assisted synthesis of pectin-stabilised CdS/ZnS core/shell nanocrystals and enhanced photocatalytic performance

Dezhi Qin[1], *Guangrui Yang*[2], *Yabo Wang*[1], *Jiajia Zhang*[1], *Li Zhang*[1] ✉

[1]*College of Chemistry and Environmental Engineering, Pingdingshan University, Pingdingshan 467000, People's Republic of China*
[2]*Institute of Environmental and Municipal Engineering, North China University of Water Resources and Electric Power, Zhengzhou 450011, People's Republic of China*
✉ *E-mail: lizhangpds@126.com*

Published in Micro & Nano Letters; Received on 25th January 2020; Revised on 16th April 2020; Accepted on 20th April 2020

Pectin-conjugated CdS/ZnS core/shell nanocrystals were prepared by using a microwave-assisted approach without the addition of any external ligands. The prepared cubic phase CdS/ZnS nanocrystals were uniform and mono-dispersed with sizes of 6–9 nm. The charge and long-chain structure of pectin molecules effectively prevented the aggregation of CdS/ZnS nanocrystals. In addition, pectin molecules have multiple functional groups, such as O–H, C=O, and COO^-, which could conjugate with the surface of samples to control the growth of CdS/ZnS nanocrystals. Thermogravimetric analysis provided evidence that the obtained products are inorganic–organic hybrid materials. Based on the analysis of ultraviolet–visible spectra, it was found that the formation of ZnS shell led to a red-shift and an enhancement of absorption of CdS/ZnS nanocrystals compared with that of CdS. Photocatalytic activity of CdS/ZnS nanocrystals was monitored by the degradation of Rhodamine B under visible light irradiation. The presence of ZnS shell inhibited photo-corrosion and photo-dissolution of CdS nanocatalyst, thus resulting in a significant enhancement of photocatalytic activity and stability.

1. Introduction: CdS with a band gap of 2.42 eV at room temperature is a typical wide direct band gap II–VI semiconductor which is widely used in the fields of sensing, imaging, photovoltaics, photodetectors, and light-emitting devices [1, 2]. Its narrow band gap and negative edge make it a promising semiconductor for organic pollutant degradation under light illumination [3]. However, the biological toxicity of CdS is a key obstacle for potential catalytic applications in environmental pollution treatment. Additionally, it is well known that photo-corrosion or photo-dissolution may occur on the surface of CdS nanocrystals in the photo-catalytic process [4]. Therefore, it is imperative to design water-soluble, non-toxic inorganic nanocrystals, which has stable optical performance during photocatalytic degradation. ZnS is considered one of the less toxic semiconductors with good photoluminescence (PL) properties [5]. The epitaxial growth of a wider band gap semiconductor such as ZnS on the surface of the chalcogenide core can improve the fluorescence efficiency and chemical stability against photo-oxidation. The findings of Cui and co-workers suggested that the enveloping of Cu:ZnSe nanocrystals with a wide gap ZnS shell decreased the probability of holes being present on the surface of nanocrystals, which could dramatically improve the photostability [6].

In recent years, the strategy of biopolymer-directed was used to prepare inorganic nanomaterials, including oxides, chalcogenide semiconductors, and metallic nanoparticles [7–13]. Multi-component nanocomposites can provide novel physical and chemical properties owing to synergistic effects or complementary [14–16]. Pectin is a natural and non-toxic heteropolysaccharide present in cell walls of plant tissues. Owing to good biocompatibility and low toxicity, pectin has been widely used in the biomedical fields, such as drug delivery, tissue engineering, and bone repairing [17]. In some cases of biosynthesis, pectin was used as a matrix to stabilise and modify inorganic nanomaterials for the removal of dyes and heavy metals in the waste-water treatment. For example, Gupta *et al.* prepared CdS nanocrystals under friendly conditions by using pectin as the coupling negotiator, and the as-prepared products have excellent optical properties [18]. Pectin-modified iron oxide magnetic nanocomposites could effectively adsorb and remove methylene blue (MB) and Cu^{2+} ions from aqueous solution [19, 20].

Microwave (MW) irradiation is emerging as a rapid and environment-friendly mode of heating for the generation of nanomaterials. Compared with traditional synthesis methods, microwave heating can greatly shorten the reaction time and the resulting products are more uniform in terms of size and composition [21]. In recent years, it has been employed to prepare semiconductor nanomaterials with excellent optical and electric properties. For example, a microwave-assisted synthesis route is established to prepare ZnSe:Cu nanocrystals with enhanced fluorescence [22]. Shen *et al.* reported a microwave-induced synthesis of Ag centre-doped CdS nanocrystals with tunable, impurity, and visible emission [23]. In these reported works, the excellent optical property could be attributed to fast homogeneous nucleation and growth by microwave heating.

In this work, we have synthesised luminescent CdS nanocrystals with the modification of pectin via the microwave-assisted method. The ZnS shell was deposited on the surface of CdS core nanocrystals under microwave irradiation in the pectin matrix. The influence of the ZnS shell on the photocatalytic activity and durability of CdS nanocrystals was systematically investigated.

2. Experimental: Pectin and Rhodamine B (RhB) were purchased from Aladdin. Pectinase was purchased from Biosharp. Analytically pure cadmium acetate, zinc acetate, and thioacetamide (TAA) were purchased from Sinopharm Chemical Regent Co., Ltd, China. All other reagents used in experiments were of analytical grade. Distilled water used in all synthesis procedures was a high purity grade with a resistivity of 18.2 MΩ cm^{-1}.

Colloidal pectin-CdS/ZnS nanocomposites were synthesised using a microwave-assisted approach. In a typical synthesis process, 0.550 g pectin was dissolved in 50 ml hot water and transferred into a 250 ml round-bottom flask. 0.333 g cadmium acetate was dissolved in 25 ml water and added into the above solution. The mixtures of pectin–Cd^{2+} were maintained with magnetic stirring at 40°C under nitrogen protection for 30 min. Then, 0.094 g TAA was dissolved in 25 ml water and added drop-wise into a

mixed solution of pectin–Cd^{2+} with vigorous stirring at 40°C. The pH value of the solution was adjusted to 6 with the addition of 1 M NaOH. The mixed solution was rapidly microwave-heated in the microwave reaction system (2450 MHz, 240 W) for 3 min, and then cooled down to room temperature naturally. Next, 0.549 g zinc acetate was dissolved in 5 ml water and injected into a freshly prepared pectin–CdS solution. After chelating of Zn^{2+} to pectin for 5 min, 0.188 g TAA was dissolved in 5 ml water and added drop-wise into as-prepared solution with vigorous stirring. The final concentration of pectin was 5 mg ml^{-1}, the molar ratio of Zn/Cd was 2:1. The reaction solution was again microwave-heated in the microwave reaction system (2450 MHz, 240 W) for 3 min, and then separated by high speed centrifuging at 12,000 rpm. The collected solid-state products were washed with distilled water and ethanol respectively, and finally dried in a vacuum at 50°C for 48 h.

Powder X-ray diffraction (XRD) characterisation was carried out on a Rigaku Smartlab diffractometer. Examinations of the morphology and composition of pectin stabilised CdS/ZnS nanocrystals by transmission electron microscopy (TEM) and energy-dispersive X-ray spectrum (EDS) made use of a JEOL JEL-2010 transmission electron microscope equipped with an X-ray energy-dispersive detector. The ultraviolet–visible (UV–Vis) spectra were measured at room temperature using a Shimadzu UV-2550 spectrophotometer. PL spectra were acquired with a Hitachi F7000 spectrophotometer. Thermogravimetric analysis (TGA) was performed with a TA Q-600 thermogravimetric apparatus. Fourier transform infrared (FTIR) spectra were recorded on a Bruker Tensor-37 spectrophotometer. The surface charges of products were determined on a Malvern Nano ZS zeta potential analyser.

The photocatalytic activity of the samples was studied for the degradation of RhB under visible irradiation (350 W Xe lamp). Photocatalyst (180 mg) was added into 150 ml of RhB aqueous solution (10^{-5} mol l^{-1}); the pH value of the solution was adjusted to 8. Before the irradiation, the suspensions were magnetically stirred to achieve the adsorption/desorption equilibrium between dye molecules and catalysts for 30 min in the dark. Then, the suspensions were exposed to visible light irradiation. At a given time interval, the remaining concentration of RhB was calibrated by examining the absorption at 554 nm in the UV–vis spectra of samples.

3. Results and discussion: The crystal structure of as-prepared samples was studied by using XRD characterisation. Fig. 1 shows the XRD patterns of pectin–CdS and pectin–CdS/ZnS nanocomposites with different Zn/Cd molar ratios. There are broad and weak diffraction peaks (10–20°) as indicated by the asterisk originating from the polymer phase in all XRD patterns, which suggests the presence of pectin polymer in the as-prepared nanocrystals. For pectin–CdS composite (Fig. 1*a*), all of the diffraction peaks can be well-indexed to the cubic phase of CdS, in close agreement with literature values (JCPDS No. 10-0454). The broadening of diffraction peaks may be attributed to the small size of the samples. From XRD patterns of pectin–CdS/ZnS (Figs. 1*b* and *c*), it is found that the Bragg reflections corresponding to ZnS or ZnO are not observed, indicating the epitaxial growth of ZnS on CdS core and further confirming the formation of CdS/ZnS core/shell structure. In addition, the diffraction peaks of CdS/ZnS nanocomposites shift slightly towards higher 2θ angles because of smaller lattice constants of ZnS; the intensity of XRD peaks increase slightly with the increase of Zn/Cd molar ratio, indicating these samples tend to be well crystallised.

Fig. 2*a* shows the TEM image of pectin–CdS nanocrystals in a typical experiment. Clearly, it can be seen that CdS particles synthesised in pectin solution are of a near-spherical shape and possess high uniformity with an average size of 4–6 nm. Since the reaction pH value is higher than the isoelectric point of pectin (~2.5), the surface of pectin was negatively charged (−26.0 mV) from zeta potential analysis. The pectin–CdS solution was also found to be negatively charged with a zeta potential of −34.1 mV, suggesting that the surface charge of CdS nanoparticles was dominated by the bound pectin molecules. Pectin molecules could absorb in the surface of CdS nanocrystals and effectively prevent aggregation due to electrostatic interaction. In addition, it was suggested by Gupta and co-workers that pectin could stabilise nanoparticles by virtue of its long-chain structure [24].

To confirm that pectin plays the role in controlling the size and morphology of CdS nanocrystals in aqueous solution, the control experiments were carried out to prepare CdS crystals with different amounts of pectin. When the concentration of pectin decreased to 1 mg ml^{-1}, the obtained products were badly aggregated and form larger particles (not shown in the figure). Lower concentration of pectin might reduce the extent of coating on CdS nanoparticles,

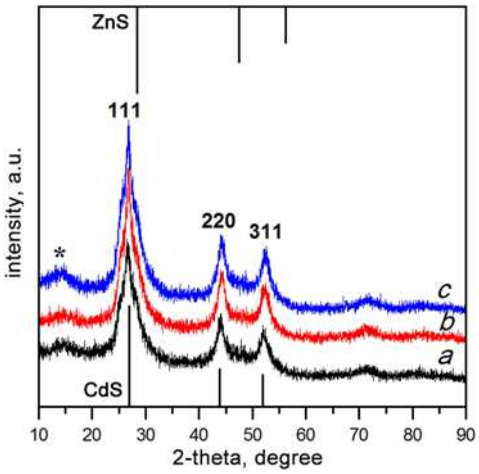

Fig. 1 *XRD patterns of as-prepared samples*
a Pectin–CdS nanocrystals
b Pectin–CdS/ZnS nanocrystals with a molar ratio of Zn/Cd = 1.25
c Pectin–CdS/ZnS nanocrystals with a molar ratio of Zn/Cd = 2

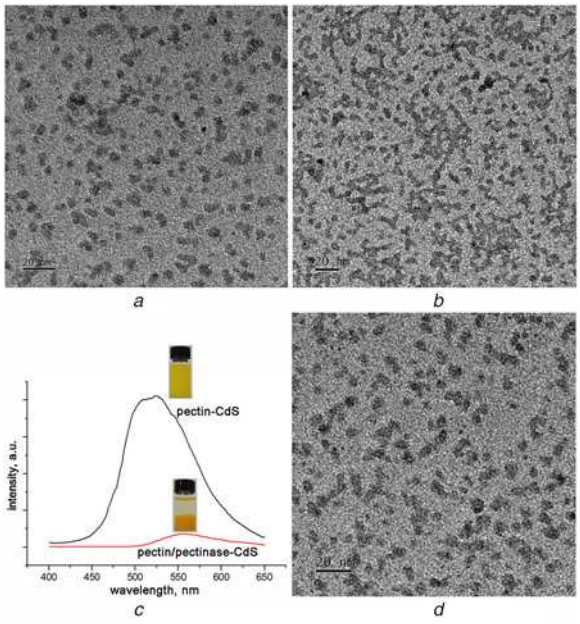

Fig. 2 *TEM images of pectin–CdS nanocrystals with different concentration of pectin*
a 5 mg ml^{-1}
b 10 mg ml^{-1}
c PL spectra of pectin–CdS and pectin/pectinase–CdS
d TEM image of pectin–CdS/ZnS nanocrystals

doi: 10.1049/mnl.2020.0062

which resulted in weak electrostatic repulsive force against the agglomeration of particles. The TEM image of CdS nanocrystals prepared in a relatively high concentration of pectin (10 mg ml^{-1}) was shown in Fig. 2*b*. It can be observed that the CdS particles are in close contact with each other to form short chains. We hypothesise that pectin aggregation is favoured at higher concentrations through hydrogen bonding between COO^- and CH_2 groups, which lead to the aggregation of several CdS nanoparticles to form chain structures. As can be seen in Fig. 2*c*, pectin-stabilised CdS nanocrystals exhibit an emission band centred at about 525 nm that arise from sulphur vacancy defects. With the addition of pectinase, the pectin–CdS solution showed obvious flocculate and most of the fluorescence was lost. This is due to the fact that pectinase can depolymerise pectin molecule by eliminating cleavage of β-glycosidic linkages, and thus pectin did not act as a template to control the morphology and size of CdS nanoparticles. As shown in Fig. 2*d*, the size of pectin–CdS/ZnS nanocrystals is slightly larger than that of CdS core; the diameter of the core/shell nanostructure is determined to be about 6–9 nm, indicating the growth of a ZnS shell outside core nanocrystals. The electrostatic interaction of pectin–CdS (negatively charged) and Zn^{2+} promotes the formation of a coordinate-covalent bond and thus reduces the nucleation activation energy of ZnS nanocrystals. The presence of cadmium, zinc, and sulphur besides that of carbon and oxygen in the EDS spectrum (Fig. 3) verifies the formation of pectin-capped CdS/ZnS nanocrystals in the powder sample.

The high-resolution TEM (HRTEM) image of the pectin-conjugated CdS/ZnS nanocrystals is shown in Fig. 4*a*, which provides further insight into the morphology of the as-prepared nanocrystals. It can be seen that there is a significant contrast on the individual nanoparticle, indicating the existence of different composition and structure in nanoparticles. We speculate that the dark part centred at each particle is CdS core and the grey part in the surface layer is ZnS shell. In addition, the edges of CdS/ZnS nanoparticles look fuzzy and amorphous, which could possibly be the pectin molecules. According to the discussion above, it is summarised that the ligands of pectin coordinate with nanoparticles, which forms a thin film on the surface to stabilise CdS/ZnS core/shell nanocrystals (Fig. 4*b*).

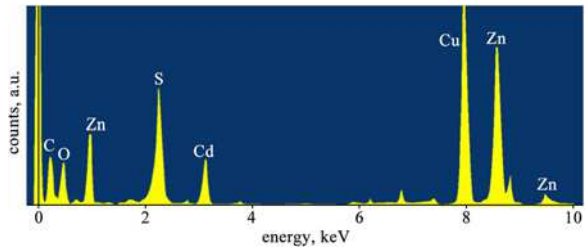

Fig. 3 *EDS spectrum of pectin–CdS/ZnS nanocrystals*

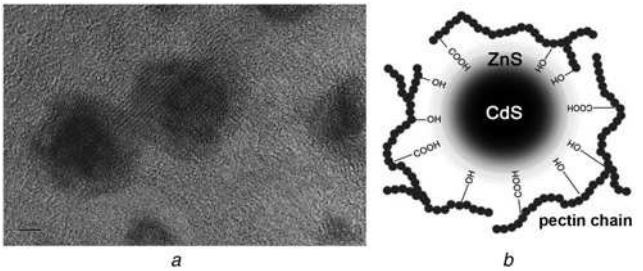

Fig. 4 *Morphology and reaction mechanism of pectin–conjugated CdS/ZnS nanocrystals*
a HRTEM image of pectin–CdS/ZnS nanocrystals
b Illustration of the interaction between pectin ligands with CdS/ZnS nanocrystals

The FTIR spectra were taken to study the interaction of CdS/ZnS nanocrystals with pectin. The IR peaks of pure pectin as shown in Fig. 5*a* at 3395, 2936, and 1736 cm^{-1} are assigned to stretching vibrations of the O–H, C–H and C=O in free carboxylic acid, respectively. Carboxylate (COO^-) groups show two bands, an asymmetrical stretching band at 1638 cm^{-1} and a symmetric stretching band at 1395 cm^{-1}. The characteristic IR peaks of pectin in the obtained products are still retained by centrifuging and washing repeatedly, suggesting the strong interaction between pectin and CdS/ZnS nanocrystals. Comparing the IR spectrum of pectin–CdS/ZnS with that of pure pectin, the peak of the O–H group shifts to a high wave number of about 11 cm^{-1}, and the IR peaks of C=O and COO^- stretching bands shift to low wave number about 6 and 16 cm^{-1}. FTIR spectra provide clear evidence that pectin molecules have multiple binding sites such as O–H, C=O to react with the surface of CdS/ZnS nanocrystals, and further regulate the growth of nanocrystals through the interfacial molecular recognition of biomolecules with inorganic materials.

For the TGA curve of pectin-conjugated CdS/ZnS nanocrystals (Fig. 5*b*), there are three stages of weight loss. The first stage of the decomposition observed up to 225°C is due to moisture evaporation and the loss of chemical bonding water. From 225 to 295°C, the loss of weight is mainly owing to the escape of several kinds of small molecules. The last stage of the weight loss from 295 to 510°C corresponds to the pyrolysis of pectin molecules. The results of FTIR and TGA show that the interaction exists between pectin and CdS/ZnS nanocrystals. It also indicates that the obtained products are inorganic–organic hybrid materials.

Fig. 6 shows the UV–Vis spectra of pectin–CdS and pectin–CdS/ZnS nanocrystals with different Zn/Cd molar ratios. The UV–Vis spectrum of pectin–CdS nanocrystals shows a broad and structureless curve with a hump at about 428 nm, which is blue-shifted from that of bulk CdS due to quantum confinement effects. No apparent absorption peaks of ZnS could be observed from UV–Vis spectra of CdS/ZnS nanocrystals, suggesting the epitaxial growth of ZnS shell on the surface of the CdS core. With the formation of ZnS shell (Zn/

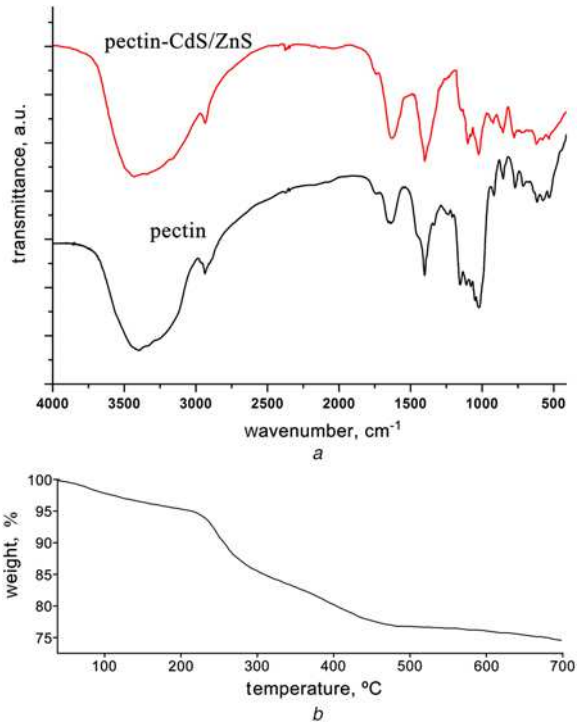

Fig. 5 *FTIR and TGA characterisation of pectin–CdS/ZnS nanocrystals*
a FTIR spectra of pectin and pectin–CdS/ZnS
b TGA analysis of pectin–CdS/ZnS

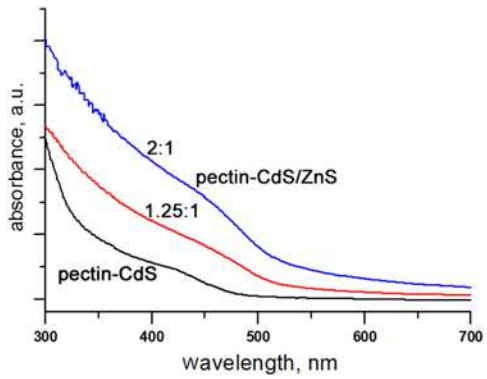

Fig. 6 *UV–Vis spectra of pectin–CdS and pectin–CdS/ZnS with different Zn/Cd molar ratios (1.25:1 and 2:1)*

Cd=1.25, 2), there are no evident variations in the absorption edge of samples, which indicates that the similar absorption mechanism of semiconductors is present in CdS/ZnS nanocrystals. The shoulder peak positions of CdS/ZnS shift to a longer wavelength compared with that of CdS nanocrystals. The band gaps calculated by means of the Tauc equation for CdS and CdS/ZnS nanocrystals are 2.79 and 2.48 eV, respectively. The growth of the ZnS shell increases the size of particles, and partial leakage of exciton into the shell matrix results in the redshift of the absorption band [25]. In addition, there is a noticeable increase of visible light absorption of samples with the formation of ZnS shell, which may lead to the higher visible light-driven photocatalytic activity.

Pectin-rich biomass such as fruit wastes and macroalgae can adsorb and remove dye molecules from water. The simultaneous adsorption and photodegradation of dye molecules is a more efficient process [19, 26]. Moreover, immobilisation of nanomaterials in the polymer matrix may be a solution for the problem with the separation of nanocatalysts from waste-water. In this work, the photocatalytic activity of the obtained products was evaluated by the degradation of RhB in aqueous solution under visible light irradiation. The RhB dye degradation rate at a different time period of Xe lamp irradiation is plotted in Fig. 7. There was no doubt that RhB dye exhibited minimum degradation under visible light irradiation without any catalysts. In contrast, 98.7% of RhB dye had degraded after 120 min Xe lamp irradiation with the presence of the CdS/ZnS nanocrystals, whereas 70.6 and 23.0% degradation were observed in the presence of CdS and ZnS nanocrystals, respectively. It can be clearly seen that CdS/ZnS has much better photocatalytic performance compared with that of pure CdS. Sabir *et al.* believed that the shell material (ZnS) has a larger band gap and both energy levels are displaced symmetrically into the core material (CdS) [27]. When the shell is excited, both electron and hole relax into the core, and thus the ZnS shell effectively passivates the surface electronic states of the CdS core, which accounts for the enhanced photocatalytic activity of CdS/ZnS core/shell nanocrystals.

The effect of photocatalyst dosage on the removal efficiency of RhB dye was studied by varying the CdS/ZnS amount (80–240 mg in 150 ml) for 10^{-5} mol l^{-1} dye solution as shown in Fig. 8. The removal rate increased with the increase of photocatalyst dosage (80–180 mg), which was attributed to the increased surface area and availability of more catalytic sites. There were no significant differences in the removal rate of dye as the photocatalyst dosage increased from 180 to 240 mg. As also depicted from Fig. 9, the removal efficiency maintained at a high level with the initial dye concentration (10^{-6} mol l^{-1}) to a threshold concentration (10^{-5} mol l^{-1}) corresponding to the saturation of the catalytic sites. In considering the removal efficiency, the photocatalyst of 180 mg and initial dye concentration of 10^{-5} mol l^{-1} were selected for our study.

The photodegradation behaviour of RhB solution over CdS/ZnS nanocrystals was observed for four cycles to evaluate the capability for reuse of catalyst, as shown in Fig. 10. The repeated photodegradation examinations demonstrated that the photocatalyst was very stable, and the photocatalytic efficiency almost remained unchanged after four cycles. In addition, the position and intensity of XRD peaks of samples had no notable differences in cycle photocatalytic tests (data not shown). It is well known that pure CdS has poor photostability and durability in the removal of organic pollutants due to the photo-corrosion and photo-dissolution [4]. In this case, the photocatalytic activity of pure CdS decreased by 19%

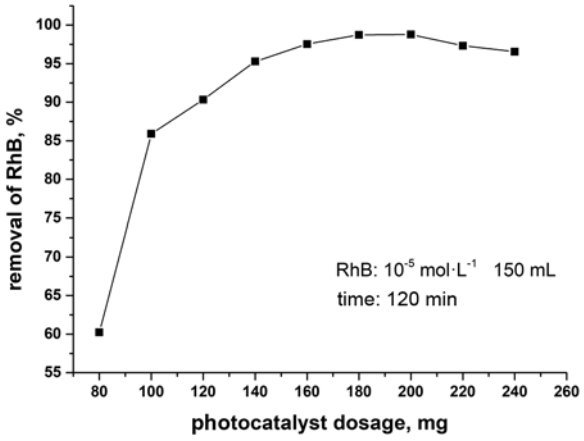

Fig. 8 *Effect of photocatalyst dosage on the removal of RhB*

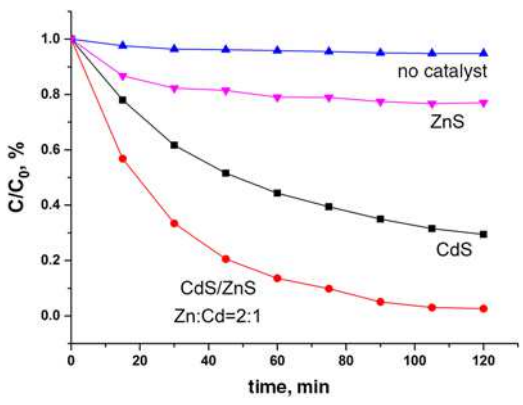

Fig. 7 *Photodegradation of RhB solution in the presence of CdS, ZnS, and CdS/ZnS nanocrystals (Zn/Cd = 2:1)*

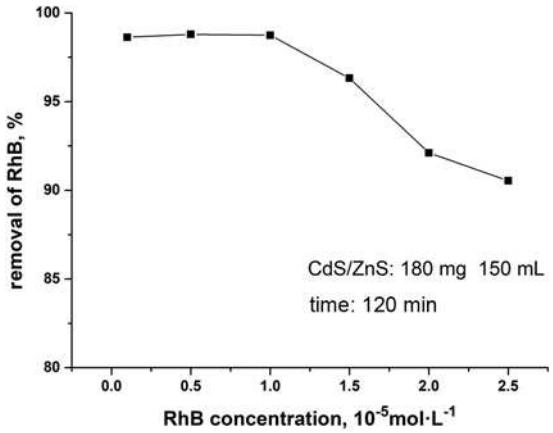

Fig. 9 *Effect of initial RhB concentration on the removal of RhB*

doi: 10.1049/mnl.2020.0062

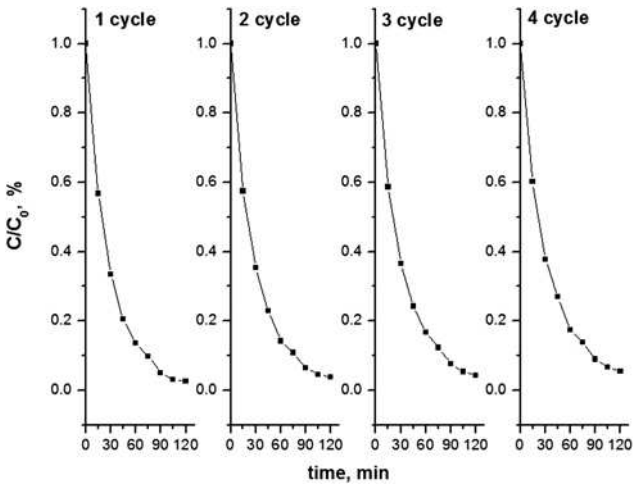

Fig. 10 *Repeated examinations of photodegradation of RhB with pectin–CdS/ZnS nanocrystals*

after four cycles. Therefore, the presence of the ZnS shell is an important factor for the improvement of the photocatalytic performance of CdS.

4. Conclusion: In summary, we have successfully synthesised pectin-stabilised CdS/ZnS core/shell nanocrystals through microwave-assisted approach in aqueous solution. The prepared cubic phase CdS/ZnS nanocrystals were uniform and monodispersed with homogeneous size. Pectin molecules could interact CdS/ZnS nanocrystals with the functional groups and conjugate the surface of nanoparticles, which played a crucial role in controlling the nucleation and growth of CdS/ZnS nanocrystals. The formation of ZnS shell on CdS core resulted in a red-shift and noticeable increase of visible light absorption, which is favoured of visible light-driven photocatalysis. The ZnS shell effectively passivated the surface electronic states of the CdS core, which promoted the separation efficiency of photo-generated electrons and holes of CdS. Therefore, the formation of the ZnS shell significantly enhanced photocatalytic activity and stability of CdS semiconductor.

5. Acknowledgments: This work was supported by the Key Project of Henan Province Higher Educational Science and Technology Program (grant no. 19B150015).

6 References

[1] Zhang B., Zheng J., Li X., *ET AL.*: 'Tuning band alignment by CdS layers using a SILAR method to enhance TiO_2/CdS/CdSe quantum-dot solar-cell performance', *Chem. Commun.*, 2016, **52**, (33), pp. 5706–5709

[2] Pinna N., Weiss K., Urban J., *ET AL.*: 'Triangular CdS nanocrystals: structural and optical studies', *Adv. Mater.*, 2001, **13**, (4), pp. 261–264

[3] Song X., Yang F., Fang Q., *ET AL.*: 'Capsule-like CdS-modified TiO_2 nanocomposites with enhanced photodegradation under visible light irradiation', *Micro Nano Lett.*, 2015, **10**, (3), pp. 157–160

[4] Yang F., Yan N.N., Huang S., *ET AL.*: 'Zn-doped CdS nanoarchitectures prepared by hydrothermal synthesis: mechanism for enhanced photocatalytic activity and stability under visible light', *J. Phys. Chem. C*, 2012, **116**, pp. 9078–9084

[5] Ahmed K.B.A., Ahalya P., Sengan M., *ET AL.*: 'Synthesis and characterization of zinc sulfide quantum dots and their interaction with snake gourd (*Trichosanthes anguina*) seed lectin', *Spectrochim. Acta A, Mol. Biomol. Spectrosc.*, 2015, **151**, pp. 739–745

[6] Wang C., Xu S., Wang Z., *ET AL.*: 'Key roles of impurities in the stability of internally doped Cu:ZnSe nanocrystals in aqueous solution', *J. Phys. Chem. C*, 2011, **115**, pp. 18486–18493

[7] Atrak K., Ramazani A., Fardood S.T.: 'Green synthesis of amorphous and gamma aluminum oxide nanoparticles by tragacanth gel and comparison of their photocatalytic activity for the degradation of organic dyes', *J. Mater. Sci., Mater. Electron.*, 2018, **29**, pp. 8347–8353

[8] Fardood S.T., Ramazani A., Joo S.W.: 'Green chemistry approach for the synthesis of copper oxide nanoparticles using tragacanth gel and their structural characterization', *J. Struct. Chem.*, 2018, **59**, pp. 482–486

[9] Fardood S.T., Ramazani A.: 'Black tea extract mediated green synthesis of copper oxide nanoparticles', *J. Appl. Chem. Res.*, 2018, **12**, pp. 8–15

[10] Fardood S.T., Ramazani A., Joo S.W.: 'Sol-gel synthesis and characterization of zinc oxide nanoparticles using black tea extract', *J. Appl. Chem. Res.*, 2017, **11**, pp. 8–17

[11] Fardood S.T., Moradnia F., Ramazani A.: 'Green synthesis and characterisation of $ZnMn_2O_4$ nanoparticles for photocatalytic degradation of Congo red dye and kinetic study', *Micro Nano Lett.*, 2019, **14**, (9), pp. 986–991

[12] Moradnia F., Ramazani A., Fardood S.T., *ET AL.*: 'A novel green synthesis and characterization of tetragonal-spinel $MgMn_2O_4$ nanoparticles by tragacanth gel and studies of its photocatalytic activity for degradation of reactive blue 21 dye under visible light', *Mater. Res. Express*, 2019, **6**, p. 075057

[13] Fardood S.T., Forootan R., Moradnia F., *ET AL.*: 'Green synthesis, characterization, and photocatalytic activity of cobalt chromite spinel nanoparticles', *Mater. Res. Express*, 2020, **7**, p. 015086

[14] Atrak K., Ramazani A., Fardood S.T.: 'Eco-friendly synthesis of $Mg_{0.5}Ni_{0.5}Al_xFe_{2-x}O_4$ magnetic nanoparticles and study of their photocatalytic activity for degradation of direct blue 129 dye', *J. Photochem. Photobiol. A, Chem.*, 2019, **382**, p. 111942

[15] Moradnia F., Fardood S.T., Ramazani A., *ET AL.*: 'Green synthesis of recyclable $MgFeCrO_4$ spinel nanoparticles for rapid photodegradation of direct black 122 dye', *J. Photochem. Photobiol. A, Chem.*, 2020, **392**, p. 112433

[16] Fardood S.T., Ramazani A., Asiabi P.A., *ET AL.*: 'A novel green synthesis of copper oxide nanoparticles using a henna extract powder', *J. Struct. Chem.*, 2018, **59**, pp. 1737–1743

[17] Kumar P.T.S., Ramya C., Jayakumar R., *ET AL.*: 'Drug delivery and tissue engineering applications of biocompatible pectin–chitin/nano $CaCO_3$ composite scaffolds', *Colloids Surf. B, Biointerfaces*, 2013, **106**, pp. 109–116

[18] Gupta V.K., Pathania D., Asif M., *ET AL.*: 'Liquid phase synthesis of pectin–cadmium sulfide nanocomposite and its photocatalytic and antibacterial activity', *J. Mol. Liq.*, 2014, **196**, pp. 107–122

[19] Rakhshaee R., Panahandeh M.: 'Stabilization of a magnetic nano-adsorbent by extracted pectin to remove methylene blue from aqueous solution: a comparative studying between two kinds of cross-likened pectin', *J. Hazard. Mater.*, 2011, **189**, pp. 158–166

[20] Gong J.L., Wang X.Y., Zeng G.M., *ET AL.*: 'Copper(II) removal by pectin–iron oxide magnetic nanocomposite adsorbent', *Chem. Eng. J.*, 2012, **185-186**, pp. 100–107

[21] Zhang J., Li C., Wang B.: 'Ag-decorated SnO_2 nanorods: microwave-assisted green synthesis and enhanced ethanol gas sensing properties', *Micro Nano Lett.*, 2017, **12**, (4), pp. 245–247

[22] Molaei M., Khezripour A.R., Karimipour M.: 'Synthesis of ZnSe nanocrystals (NCs) using a rapid microwave irradiation method and investigation of the effect of copper (Cu) doping on the optical properties', *Appl. Surf. Sci.*, 2014, **317**, pp. 236–240

[23] Shen Q., Liu Y., Xu J., *ET AL.*: 'Microwave induced center-doping of silver ions in aqueous CdS nanocrystals with tunable, impurity and visible emission', *Chem. Commun.*, 2010, **46**, pp. 5701–5703

[24] Tummalapalli M., Deopura B.L., Alam M.S., *ET AL.*: 'Facile and green synthesis of silver nanoparticles using oxidized pectin', *Mater. Sci. Eng. C*, 2015, **50**, pp. 31–36

[25] Xu S., Wang C., Wang Z., *ET AL.*: 'Aqueous synthesis of internally doped Cu:ZnSe/ZnS core-shell nanocrystals with good stability', *Nanotechnology*, 2011, **22**, (27), p. 275605

[26] Gupta V.K., Pathania D., Agarwal S., *ET AL.* 'Adsorptional photocatalytic degradation of methylene blue onto pectin–CuS nanocomposite under solar light', *J. Hazard. Mater.*, 2012, **243**, pp. 179–186

[27] Qutub N., Pirzada B.M., Umar K., *ET AL.*: 'Synthesis, characterization and visible-light driven photocatalysis by differently structured CdS/ZnS sandwich and core–shell nanocomposites', *Physica E*, 2015, **74**, pp. 74–86